Journal of Materials Chemistry

Cite this: J. Mater. Chem., 2012, 22, 11629

www.rsc.org/materials

PAPER

High performance aniline vapor detection based on multi-branched fluorescent triphenylamine-benzothiadiazole derivatives: branch effect and aggregation control of the sensing performance†

Liqi Shi,[ab] Chao He,[ab] Defeng Zhu,[a] Qingguo He,*[a] Yang Li,[c] Yan Chen,[c] Yuxi Sun,[d] Yanyan Fu,[a] Dan Wen,[ab] Huimin Cao[a] and Jiangong Cheng*[a]

Received 15th February 2012, Accepted 4th April 2012
DOI: 10.1039/c2jm30933e

A series of benzothiadiazole-pyridine branched triphenylamine derivatives TPA1BP, TPA2BP and TPA3BP have been designed and synthesized to sense aniline vapor with distinguished sensitivity, selectivity and repeatability *via* photoinduced electron transfer (PET). Suitable energy levels ensure the high selectivity to aniline for all three sensory materials. However, the aggregations of the three materials in the film state on a quartz substrate increase along with the branches, which highly deteriorate the sensing performance for less efficient fluorescence, lower contact area and inferior vapor penetration. The oriented ZnO nanorod array is introduced as the substrate to eliminate the aggregation and enhance the sensing performance, because of its high surface-to-volume ratio and 3D structure. Therefore, the cooperative effect that the sensing performance of TPA*n*BP increases with the number of branches could be observed; fluorescence intensities of the films on the nano-substrate are 34%, 45% and 54% quenched for TPA1BP, TPA2BP and TPA3BP, respectively, after exposure to 300 ppm aniline vapor for less than 5 s. Moreover, the fluorescences of all three sensory materials are almost 100% recovered by eluting with fresh air for 20 s and could be reused immediately. The detection limits are predicted to be 1 ppm for TPA1BP, 100 ppb for TPA2BP and 1 ppb for TPA3BP according to the fitted plot, demonstrating a significant cooperative effect of the molecular branches.

1. Introduction

The detection of organic amines has received more attention recently as many amines have been considered as pollutants and as toxic to human health.[1–7] Aniline and its derivatives are widely used in manufacturing dyes, rubber and agrochemicals, and exposure to aniline is suspected to result in carcinogenicity.[8,9] Thus, numerous analytical procedures have been developed for the detection of aniline and its derivatives, including spectrometry,[10,11] chromatography[12–15] and electrochemistry[16–18] methods. Though many of them have had much success, most of them suffer from time-consuming and tedious sample pre-workup such as pre-concentration of the samples by extraction. Fluorescent chemosensors have great advantages over other methods due to their high sensitivity, easy performance and fast response that are capable for real-time monitoring.[19] These fluorescent chemosensors are mostly based on fluorescence quenching or the recovery of the active materials by interaction with analytes. Many fluorescent sensors utilizing polymers or small molecules as active materials have been developed such as explosive sensors,[20,21] ion sensors[22,23] and biomolecule sensors.[24,25] However, it was seldom reported on fluorescent chemosensors which are capable of the real-time detection of volatile aniline with excellent sensitivity, selectivity and reversibility.[26–29]

In this contribution, we report on a series of sensory materials with a donor–acceptor (D–A) conjugated structure for aniline vapor detection, which is based on fluorescence quenching *via* the mechanism of PET from aniline to the sensory material. The as-synthesized compounds (TPA*n*BP, $n = 1, 2, 3$, Scheme 1) had triphenylamine (TPA) as the core and benzothiadiazole-pyridine (BP) as branch substitutes. 2,1,3-Benzothiadiazole (BT) has been widely used in various optoelectronic materials to tune the HOMO–LUMO levels and the energy gap, owing to its electron-withdrawing capability.[30–36] Here, the TPA and BP unit were coupled into one molecule to tune the energy levels and make it qualify for the PET process. The survey of the branched structure

[a]*State Key Lab of Transducer Technology, Shanghai Institute of Microsystem and Information Technology, Chinese Academy of Sciences, Changning Road 865, Shanghai 200050, China. E-mail: hqg@mail.sim.ac.cn; jgcheng@mail.sim.ac.cn; Fax: + 86 21 62511070 8934; Tel: + 86 21 62511070 8936*
[b]*Graduate School of the Chinese Academy of Sciences, Yuquan Road 19, Beijing 100039*
[c]*School of Environmental Science and Engineering, DongHua University, Yanan Road 1882, Shanghai 200051, China*
[d]*Research center of New Energy & Materials, Mianyang Normal University, Mianyang 621000, P.R. China*
† Electronic supplementary information (ESI) available. See DOI: 10.1039/c2jm30933e

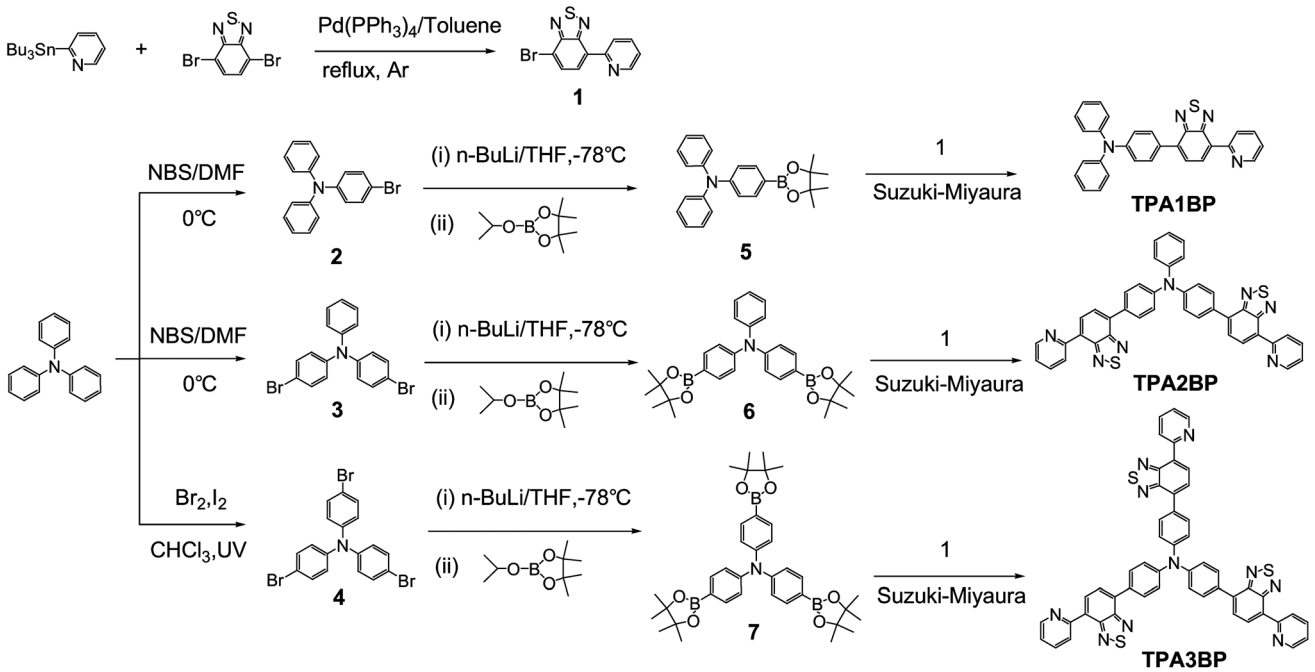

Scheme 1 Synthetic routes for TPA*n*BP (n = 1, 2, 3).

lies in two aspects. Firstly, the electrons could delocalize over all conjugated branches in such multi-branched D–A structures across the central TPA unit, which leads to cooperative effects such as increased two-photon absorption cross section and electroluminescence performance.[37–39] For fluorescent sensory materials, the cooperative effects of multi-branched structures may also amplify the quenching signal compared with its mono-branched counterparts. Secondly, the branch effect may be designed to control the morphology of the film sensor and deepen the understanding of the relationship between molecular aggregation and sensing properties. More conjugated branches may lead to different intermolecular packing modes in the solid state as they tend to form an amorphous state with more branches.[40] The packing mode may play a critical role in its sensory performance since the sensing process requires a large contact area and a suitable interaction distance to enhance the efficiency of electron transfer. In the film state, serious self-aggregation may also cause poor vapor penetration, a small contact area and low fluorescence intensity.

All of the three compounds TPA*n*BP (n = 1, 2, 3) showed strong fluorescence both in solution and in film state, and the fluorescence could be quenched upon exposure to aniline vapor. The high selectivity to aniline was demonstrated and attributed to the appropriate energy levels for electron transfer from aniline to the photoexcited state of TPA*n*BP. Furthermore, introducing a nano-structure as the film substrate could effectively inhibit the multi-branch induced aggregation, as well as bringing about a fast response (within 5 s) and high reversibility (almost 100% reversible by eluting with air for less than 20 s) to aniline vapor for all three sensory materials. Moreover, the sensory performance, especially the limit of detection, exponentially increased along with the branches, indicating the strong cooperativity of the branches; namely, TPA3BP showed the best sensory performance for aniline detection with a limit as low as 1 ppb.

2. Results and discussion

2.1. Synthesis

The synthetic procedure was illustrated in Scheme 1. Compound **1** was obtained from the Stille coupling of 2-(tributylstannyl) pyridine and 4,7-dibromo-2,1,3-benzothiadiazole in 27% yield. NBS and Br_2 were used to brominate triphenylamine (TPA), affording **2**, **3** and **4** in yields of 91%, 88% and 66%, respectively. Compounds **2**, **3** and **4** were subjected to halogen–lithium exchange and the subsequent reaction with 2-isopropoxy-4,4,5,5-tetramethyl-1,3,2-dioxaborolane to give **5**, **6** and **7** in 68%, 47% and 57% yield, respectively. Suzuki–Miyaura cross-coupling of 1 and 5 resulted in TPA1BP (yield, 73%). Similar reactions of **6** and **7** with **1** yielded compounds TPA2BP (38.5%) and TPA3BP (55.4%), respectively. The chemical structures of all compounds were verified using ^{1}H NMR spectroscopy and MALDI-TOF mass spectrometry. The detailed synthetic route is summarized in the supporting information.†

2.2. Optical and electrochemical properties

The absorption and emission spectra of TPA*n*BP (n = 1, 2, 3) in both solution and film were illustrated in Fig. 1, and the data were summarized in Table 1. The spectra of the three materials were all normalized to the maximum absorption or emission intensity of TPA3BP whether in solution or film state. In Fig. 1a, the absorbance of the three materials increased along with the number of BP units both in solution (intensity ratio, 1 : 2 : 3) and in film (1 : 1.4 : 1.9), suggesting that the molar extinction coefficient increased by introducing more BP units into the one molecule. In the film state, the absorption peaks of the three materials red shifted by 16, 20 and 23 nm compared to those of their solution states, indicating that molecular aggregation occurred in the films and the aggregation tended to be more

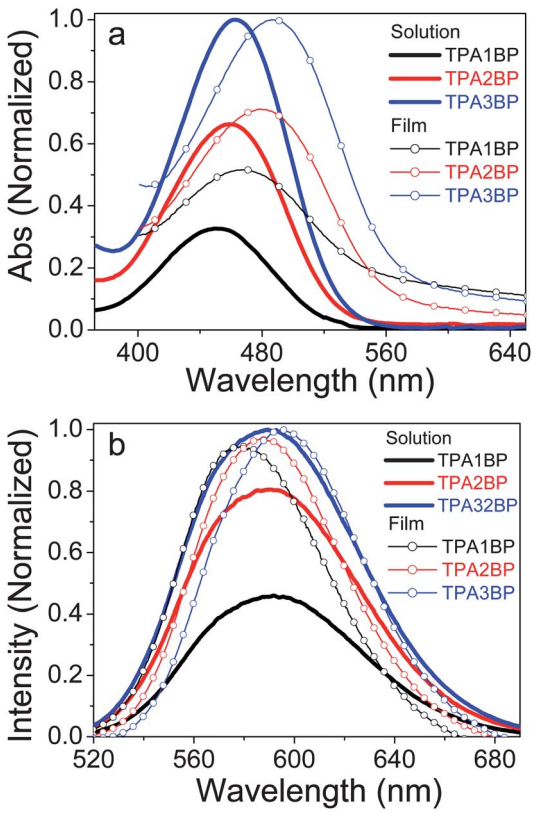

Fig. 1 UV-vis absorption (a) and emission (b) spectra of TPA*n*BP (n = 1, 2, 3) in chloroform solution (1×10^{-5} M) and film. The films were spin-casted from their chloroform solution. The spectra of the three compounds in (a) and (b) were measured under the same conditions.

severe with more branches. The emission intensity of TPA*n*BP (n = 1, 2, 3) in solution increased (1 : 1.7 : 2.2, shown in Fig. 1b) due to the successively enhanced extinction coefficient (Table 1). However, in the film state, TPA*n*BP showed comparable emission intensities, indicating that aggregation took place with the increase of branches. The detailed morphology effect was discussed in the following investigation.

The electrochemical behavior of TPA*n*BP (n = 1, 2, 3) was characterized and their cyclic voltammetric curves were shown in Fig. S1.† The onset oxidation/reduction potentials of TPA*n*BP (n = 1, 2, 3) were estimated to be 0.92/−1.32V, 0.94/−1.31V and 0.96/−1.30V *vs.* SCE, respectively. The HOMO/LUMO energy levels and energy bandgap (E_g) of the three compounds were calculated as shown in Table 1.

2.3. Sensory properties

Fig. 2 showed the energy levels and Stern–Volmer plots of TPA*n*BP for different amines.[4a,41] The HOMO levels of TPA*n*BP were all slightly lower than that of aniline, which ensured the PET from aniline to TPA*n*BP. The PET from aniline to the photoexcited state of TPA*n*BP resulted in fluorescence quenching. However, for other amines, such as triethylamine, hexylamine, cyclohexylamine, benzylamine and *p*-nitroaniline, their HOMO energy levels were lower than that of TPA*n*BP, therefore no fluorescence quenching was found. It should be noted that the PET between *p*-methylaniline and TPA*n*BP led to a much lower quenching efficiency in contrast to aniline, which might be attributed to its much higher HOMO level. The selective optical response of TPA*n*BP ensured its application in aniline detection.

Fig. 3 illustrated the fluorescence responses of TPA*n*BP (n = 1, 2, 3) to aniline vapor in the film state on quartz substrate. TPA1BP showed a much higher quenching efficiency than TPA2BP and TPA3BP. About 35% of the fluorescence of TPA1BP is quenched after the first 10 s of exposure to saturated vapor of aniline (860 ppm) and it increased to 50% upon further exposure for 50 s. However, TPA2BP and TPA3BP gave similar quenching efficiencies which are only 8% quenched within the first 10 s, and increased to 24% and 27% with further exposure for 50 s, respectively. As the energy levels and molecular structures of TPA*n*BP are similar, the decreased quenching efficiency from TPA1BP to TPA3BP could arise from the morphology difference of the films.

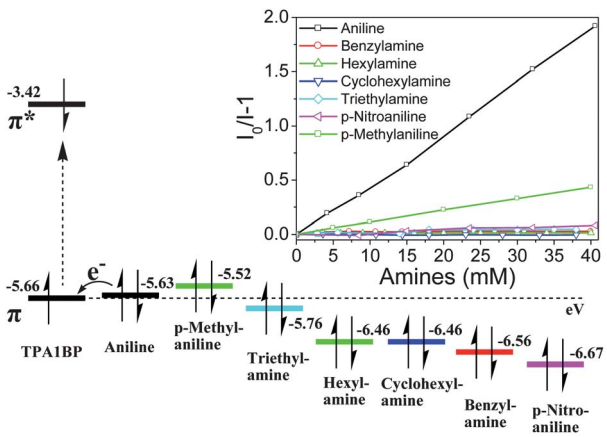

Fig. 2 HOMO (π) and LUMO (π*) energy levels of TPA1BP and different amines. The inset shows the Stern–Volmer plots of TPA1BP (10^{-4} M in THF) in the presence of different amines.

Table 1 Optical and electrochemical properties of TPA*n*BP (n = 1, 2, 3)

	Abs[a], λ_{max}/nm		PL[a], λ_{max}/nm					
	Solution	Film	Solution	Film	HOMO[b]/eV	LUMO[b]/eV	E_g[b]/eV	Φ
TPA1BP	450	466	591	576	−5.66	−3.42	2.24	0.51
TPA2BP	459	479	591	586	−5.68	−3.43	2.25	0.50
TPA3BP	463	486	591	595	−5.70	−3.44	2.26	0.55

[a] The excitation light wavelength was at 460 nm, and the films were spin-casted from their chloroform solution on a quartz plate. [b] HOMO = $-e(E_{ox}^{onset} + 4.741)$ (eV), LUMO = $-e(E_{red}^{onset} + 4.741)$ (eV), E_g = LUMO − HOMO.

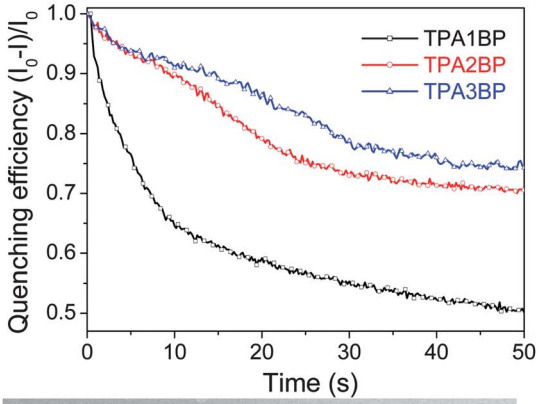

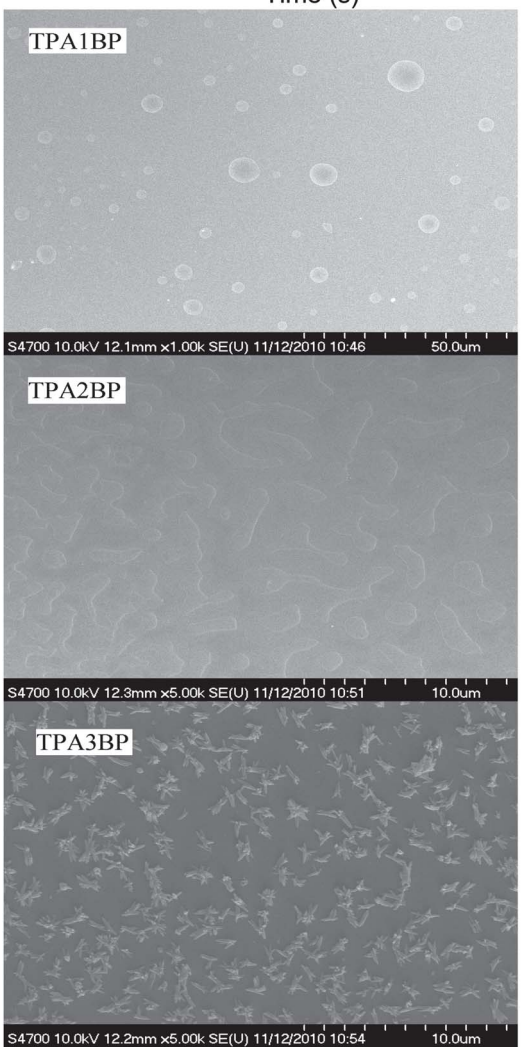

Fig. 3 The time-course fluorescence responses of TPA*n*BP (n = 1, 2, 3) films on quartz to aniline saturated vapor at 25 °C and their corresponding SEM images.

These morphology differences were investigated by scanning electron microscopy (SEM) images of TPA*n*BP (n = 1, 2, 3) coated from their chloroform solutions (7×10^{-4} M). The SEM image showed that on a quartz substrate, TPA1BP formed a relatively smooth film except for a few points of imperfection. TPA2BP became separated lumps and triple-branched TPA3BP evolved into nano-sticks with a diameter of ~200 nm. The severe aggregations in TPA2BP and TPA3BP were attributed to the increase of the BP units which caused strong intermolecular interactions *via* heteroatom contacts and/or π–π interactions of the thiadiazole-containing compounds. That is, the increased self-aggregation from TPA1BP to TPA3BP not only resulted in the low fluorescence intensity as we discussed above, but also induced a poor sensory response due to poor vapor penetration and a small contact area of the sensory films.

To eliminate the aggregation of the as-prepared film sensor, a nano-structured substrate was introduced since its high area-to-volume ratio could ensure the good dispersion and de-aggregation of the TPA*n*BP molecules and provide more contact sites for the sensory materials.[42,43] Besides, as we reported recently, nanorod arrays could bring about a significant enhancement of the fluorescence intensity and sensing performance for their optical modulation of the nanorod waveguide.[43]

In this work, the sensor device was fabricated by a simple spin-coating of TPA*n*BP solution onto the vertically oriented ZnO nanorods arrays (~1.2 μm height, possessing uniform nanorods of ~80 nm in diameter). Here, the same concentrations of TPA*n*BP (n = 1, 2, 3) were taken as those used on the quartz substrate. As shown in Fig. 4, all structures exhibited uniform verticality, enough voids and a smooth surface, which ensured high efficient light transmission and quick diffusion of vapor molecules. No obvious morphological differences could be found after coating. In particular, no aggregation of TPA3BP appeared with the introduction of nanorod arrays, which strongly supports our assumption. Top-view images were presented in Fig. S2.†

Fig. 5 presented the real time-course fluorescence responses of TPA*n*BP (n = 1, 2, 3) films on nano-substrates to aniline vapors of different concentrations. As expected, TPA*n*BP (n = 1, 2, 3) films on the nano-substrates displayed very fast responses and were almost 100% reversible to aniline vapor in Fig. 5a. In contrast to the best sensory performance of Fig. 3 that only 50% was quenched after exposure to 860 ppm aniline vapor for 50 s, the fluorescence of the film on the nano-substrate was 34%, 45% and 54% quenched for TPA1BP, TPA2BP and TPA3BP after exposure to 300 ppm aniline vapor for less than 5 s, respectively. This result indicated that the aggregation could be controlled by introducing the ZnO nanorod array. The increased BP unit of TPA2BP and TPA3BP is advantageous for the enhanced sensitivity. Quantum-chemical calculations (Fig. S3†) indicated that the electrons in the HOMO orbital delocalized across the three

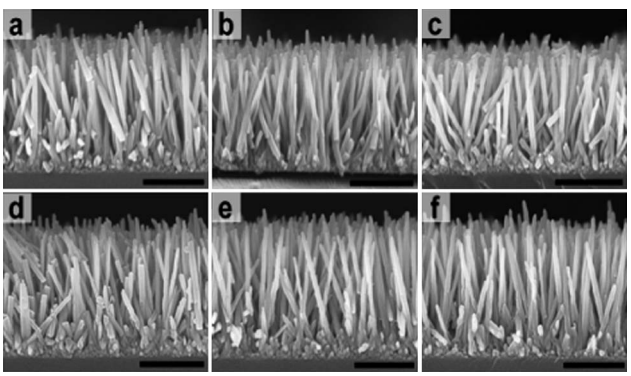

Fig. 4 Cross-view images of the nanorod structures (a–c) before and (d–f) after TPA*n*BP (n = 1, 2, 3) coating (scale bar is 1 μm).

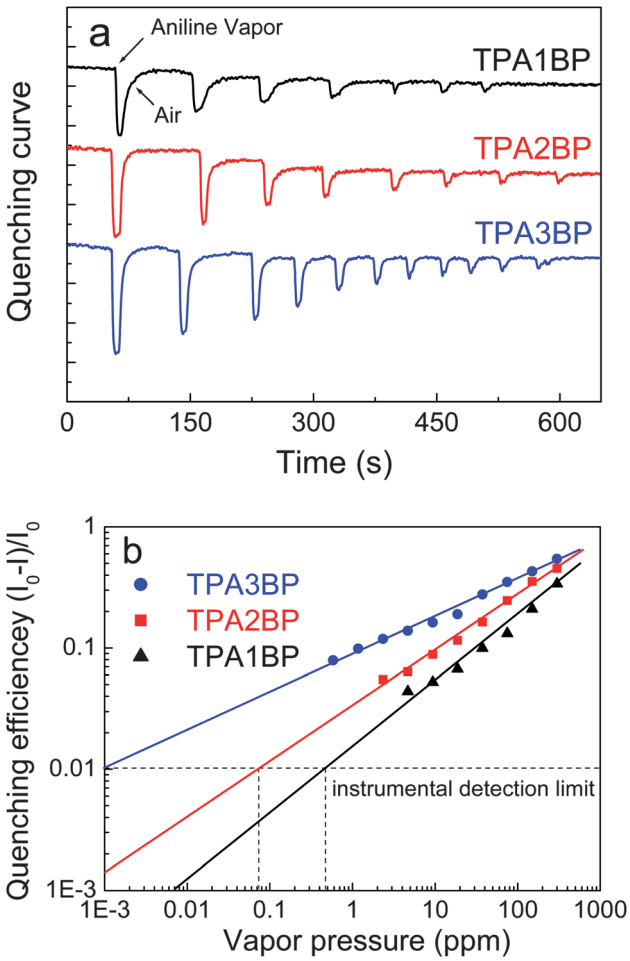

Fig. 5 (a). Time-course fluorescence responses of TPA*n*BP ($n = 1, 2, 3$) films on nano-substrates to the different concentrations of aniline vapor: all the first exposures were at 300 ppm, after elution with air, the next exposure was at a half-diluted concentration of the previous vapor. All the emission intensities were monitored at 570 nm. (b) Fluorescence quenching efficiency ($1 - I/I_0$) as a function of the vapor pressure of aniline, fitted with the Langmuir equation.

branches, except for the pyridyl part, proving that the cooperative effect would contribute to the enhanced sensitivity in TPA3BP. Moreover, the fluorescence of all the sensory films was almost 100% recovered by eluting with air for 20 s and the recovered film sensor could be reused immediately.

To determine the detection limit, the aniline vapor was diluted with air every time by half in the subsequent continuous sensing test, and the fluorescence quenching efficiency of TPA*n*BP ($n = 1, 2, 3$) as a function of the vapor pressure of aniline was illustrated, as shown in Fig. 5b. The quenching data of each film sensor is well-fitted by the Langmuir equation and the detection limit can be extrapolated to be ~1 ppm for TPA1BP, ~100 ppb for TPA2BP and ~1 ppb for TPA3BP according to the fitted plot, if the triple multiple signal to noise ratio of the fluorescent detection device was considered as 0.01. Whereas, in the latest reports, a well-calibrated photodetector can detect intensity changes as low as 0.1%,[4a,4b] the detection limit of TPA3BP could be determined as 1 ppt. Such a 10 and 100 fold detection limit difference from TPA1BP to TPA3BP means a significant cooperative

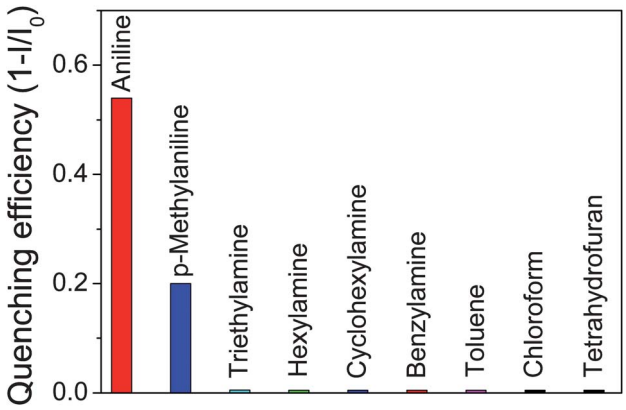

Fig. 6 Fluorescence responses of the TPA3BP films on nano-substrates after exposure to 300 ppm of various amines and solvent vapors for 5 s.

branch effect existed in the branched sensing system. The selectivity test proved that other amines and common solvent vapors (Fig. 6) caused no quenching for all the sensory devices.

4. Conclusions

In summary, three benzothiadiazole-pyridine branched triphenylamine derivatives have been synthesized and characterized for aniline sensing. The HOMO/LUMO levels of the molecules were tuned to achieve a selective PET from aniline to the analytes. All of the three compounds showed strong fluorescence with a quantum efficiency as high as ~0.5 in solution. However, with the increase of the BP moiety, severe aggregation in the film occurred, which retards the vapor penetration and decreases the active contact area. A nano-structured substrate was used to decrease the aggregation and increase the sensing performance. TPA3BP showed a 100 and 1000 fold decreased limit of detection over its bi-branched and mono-branched counterparts to aniline vapor when casted on a nano-structure for its multi-branched structure. A significant improvement of the sensory property, attributed to the controlled aggregation *via* the nano-structured substrate, also suggests that besides the molecular structure, morphology control is considered more important in sensory material and device design. The designed and synthetic strategy presents a simple and practical approach to construct fluorescence chemosensors for environmental pollutant detection and monitoring.

Experimental

Synthesis

4-Bromo-7-(2-pyridinyl)-2,1,3-benzothiadiazole (1). A 250 mL three-necked round-bottomed flask was charged with 4,7-dibromo-2,1,3-benzothiadiazole (4.8 g, 16.3 mmol) and $Pd(PPh_3)_4$ (0.95 g, 0.82 mmol) under argon, then a toluene solution (120 mL) of 2-(tributylstannyl)pyridine (6 g,16.25 mmol) was added. The reaction mixture was heated to reflux at 117 °C and stirred for 12 h. After being cooled to room temperature, the mixture was washed with saturated aqueous NaCl (100 mL) and the organic layer was separated and dried over anhydrous $MgSO_4$. The solvent was removed and the

residue was purified by column chromatography to afford a yellow solid (1.28 g, 27%). ^{1}H NMR (500 M, $CDCl_3$, ppm) δ 8.77 (d, 1H, $J = 4$ Hz), 8.63 (d, 1H, $J = 7.5$ Hz), 8.36 (d, 1H, $J =$ 8 Hz), 8.00 (d, 1H, 7.5Hz), 7.87 (m, 1H), 7.26 (m, 1H); MALDI-TOF MS: *m/z* 292.

4-Bromotriphenylamine (2). A solution of NBS (3.63 g, 20.4 mmol) in DMF (40 mL) was added dropwise into a solution of triphenylamine (5.0 g, 20.35 mmol) in DMF (60 mL), and then stirred at 0 °C for 4 h. The solvent was removed, the residue was washed with water (150 mL) and saturated aqueous NaCl (100 mL), and the organic layer was dried over anhydrous $MgSO_4$. Then the solvent was removed and the residue was purified by silica gel chromatography eluted with petroleum ether to get pellucid liquid (6 g, 91%). ^{1}H NMR (500 M, $CDCl_3$, ppm) δ 7.31 (d, 2H, $J = 8.5$ Hz), 7.24 (t, 4H, 7.5Hz), 7.07 (d, 4H, $J = 8$ Hz), 7.02 (t, 2H, J = 7.5HZ), 6.93 (m, 2H); MALDI-TOF MS: *m/z* 323.

4,4′-(Dibromo)triphenylamine (3). A solution of NBS (7.26 g, 40.8 mmol) in DMF (80 mL) was added dropwise into a solution of triphenylamine (5.0g, 20.35 mmol) in DMF (60 mL), and then stirred at 0 °C for 4 h. The solvent was removed, the residue was washed with water (150 mL), saturated aqueous NaCl (100 mL), and the organic layer was dried over anhydrous $MgSO_4$. Then the solvent was removed and the residue was purified by silica gel chromatography eluted with petroleum ether to get pellucid liquid (7.2 g, 88%). ^{1}H NMR (500 MHz, $CDCl_3$, ppm) δ 7.31 (m, 4H), 7.24 (m, 2H), 7.05 (m, 3H), 6.91 (m, 4H); MALDI-TOF MS: *m/z* 400.9.

4,4′,4″-(Tribromo)triphenylamine (4). A 250 mL three-necked round-bottomed flask charged with triphenylamine (5.0120 g, 20.4 mmol), and chloroform (100 mL). A solution of Br_2 (3.25 mL, 0.0634 mol) in chloroform (20 mL) was added dropwise under UV irradiation. The reaction solution turned from purple red to green. The reaction solution was stirring at room temperature for 24 h under UV irradiation. Then the mixture was extracted with $CHCl_3$ (30 mL), and washed with NaOH (2 M aq) and water. The organic layer was separated and dried over anhydrous $MgSO_4$. The solvent was removed and the residue was pre-purified by column chromatography eluted with chloroform and followed by recrystallization in hexane to get a pellucid solid (6.45 g, 66%). ^{1}H NMR (500 MHz, $CDCl_3$, ppm) δ 7.34 (m, 6H), 6.91 (m, 6H); MALDI-TOF MS: *m/z* 478.8.

4-(4,4,5,5-Tetramethyl-1,3,2-dioxaborolan-2-yl)triphenylamine (5). To a THF solution of **2** (2 g, 6.2 mmol), *n*-BuLi (5 mL, 0.88 g, 14 mmol) was added under argon and stirring for 1 h at −78 °C, then 2-isopropoxy-4,4,5,5-tetramethyl-1,3,2-dioxaborolane (2.8 mL, 2.55 g, 13.6 mmol) was added dropwise, after stirring at this temperature for 1 h, the mixture was cooled to room temperature and reacted for 12 h. The mixture was quenched with water (20 mL) and extracted with $CHCl_2$, and the organic layer was dried over anhydrous $MgSO_4$. The solvent was removed and the residue was pre-purified by column chromatography followed by recrystallization in methanol to get a white solid (1.56 g, 68%). ^{1}H NMR (500 MHz, $CDCl_3$, δ (ppm)) δ 7.65 (d, 2H, 8.5Hz), 7.23 (m, 4H), 7.09 (d, 4H, $J = 7.5$ Hz), 7.01 (m, 4H); MALDI-TOF MS: *m/z* 371.

4,4′-(Bis(4,4,5,5-tetramethyl-1,3,2-dioxaborolan-2-yl))triphenylamine (6). To a THF solution of **3** (2 g, 5 mmol), *n*-BuLi (7 mL, 19.6 mmol) was added under argon and stirred for 1 h at −78 °C; then 2-isopropoxy-4,4,5,5-tetramethyl-1,3,2-dioxaborolane (4.4 mL, 4.0 g, 21.36 mmol) was added dropwise. After stirring at this temperature for 1 h, the mixture was cooled to room temperature and reacted for 12 h. The mixture was quenched with water (20 mL) and extracted with $CHCl_2$, and the organic layer was dried over anhydrous $MgSO_4$. The solvent was removed and the residue was pre-purified by column chromatography followed by recrystallization in methanol to afford a white solid (1.15 g, 47%). ^{1}H NMR (500 MHz, $CDCl_3$, ppm) δ 7.66 (d, 4H, $J = 8.35$ Hz), 7.27 (s, 1H), 7.24 (s, 1H), 7.09 (d, 3H, $J = 7.8$ Hz), 7.04 (d, 4H, $J = 8.45$ Hz), 1.33 (s, 24H); MALDI-TOF MS: *m/z* 497.2.

4,4′,4″-(Tri(4,4,5,5-tetramethyl-1,3,2-dioxaborolan-2-yl))triphenylamine (7). To a THF solution of **4** (2.0g, 4.2 mmol), *n*-BuLi (1.54 g, 24.5 mmol) was added under argon and stirring for 1 h at −78 °C, then 2-isopropoxy-4,4,5,5-tetramethyl-1,3,2-dioxaborolane (5.5 mL, 5.0 g, 26.7 mmol) was added dropwise. After stirring at this temperature for 1 h, the mixture was cooled to room temperature and reacted for 12 h. The mixture was quenched with water (20 mL) and extracted with $CHCl_2$, and the organic layer was dried over anhydrous $MgSO_4$. The solvent was removed and the residue was purified by recrystallization in methanol to afford a white solid (1.5g, 57%). ^{1}H NMR (500 MHz, $CDCl_3$, ppm) δ 7.67 (d, 6H, $J = 8.45$ Hz), 7.06 (d, 6H, $J =$ 8.45 Hz), 1.34(s, 36H); MALDI-TOF MS: *m/z* 623.4.

4-(4-(Pyridine-2-yl)-2,1,3-benzothiadiazol-7-yl)triphenylamine (TPA1BP). To a flask of **5** (0.5 g, 1.3 mmol), **1** (400 mg, 1.37 mmol) and $Pd(PPh_3)_4$ (20 mg, 0.017 mmol), saturated aqueous K_2CO_3 (1 mL) and toluene (20 mL) were injected under argon. The mixture was heated to reflux for 48 h. After being cooled to room temperature, the mixture was washed with water (40 mL), and extracted with CH_2Cl_2 (100 mL). The organic layer was separated and dried over anhydrous $MgSO_4$. The solvent was removed and the residue was purified by recrystallization in methanol to afford a red solid (449 mg, 73%). ^{1}H NMR (500 MHz, $CDCl_3$, ppm) δ 8.79 (d, 1H, $J = 4.5$ Hz), 8.69 (d, 1H, 7.5Hz), 8.52 (d, 1H, 7.5Hz), 7.87 (m, 3H), 7.83 (d, 1H, $J = 7.5$ Hz), 7.33 (m, 1H), 7.28 (m, 4H), 7.19 (m, 6H), 7.06 (t, 2H, $J = 7.5$ Hz); MALDI-TOF MS: *m/z* 456.

4,4′-(Bis(4-(pyridine-2-yl)-2,1,3-benzothiadiazol-7-yl))triphenylamine (TPA2BP). To a flask of **6** (0.2 g, 0.41 mmol), **1** (270 mg, 0.93 mmol) and $Pd(PPh_3)_4$ (20 mg, 0.017 mmol), saturated aqueous K_2CO_3 (1 ml) and toluene (20 mL) were injected under argon. The reaction mixture was heated to reflux for 48 h. After being cooled to room temperature, the mixture was washed with water (40 mL), and extracted with CH_2Cl_2 (100 mL). The organic layer was separated and dried over anhydrous $MgSO_4$. The solvent was removed and the residue was purified by recrystallization in methanol to afford a red solid (103 mg, 38.5%). ^{1}H NMR (500 MHz, $CDCl_3$, ppm) δ 8.79 (d, 2H, $J =$ 4.65 Hz), 8.69 (d, 2H, $J = 8$ Hz), 8.53 (d, 2H, $J = 7.45$ Hz), 7.95 (d, 4H, $J = 8.6$ Hz), 7.86 (m, 4H), 7.29 (m, 10H), 7.12 (t, 1H, $J =$ 7.25 Hz); MALDI-TOF MS: *m/z* 667.1.

4,4′,4″-(Tri(4-(pyridine-2-yl)-2,1,3-benzothiadiazol-7-yl))triphenylamine (TPA3BP). To a flask of **7** (0.2 g, 0.32 mmol), **1** (326mg, 1.12 mmol) and $Pd(PPh_3)_4$ (20 mg, 0.017 mmol), saturated aqueous K_2CO_3 (1 mL) and toluene (20 mL) were injected under argon. The reaction mixture was heated to reflux for 48 h. After being cooled to room temperature, the mixture was washed with water (40 mL), and extracted with CH_2Cl_2 (100 mL). The organic layer was separated and dried over anhydrous $MgSO_4$. The solvent was removed and the residue was purified by recrystallization in methanol to afford a red solid (155 mg, 55.4%). ^{1}H NMR (500 MHz, $CDCl_3$, ppm) δ 8.81 (d, 3H, J = 4 Hz), 8.71 (d, 3H, J = 8 Hz), 8.56 (d, 3H, J = 7.5 Hz), 8.01 (d, 6H, J = 8.65 Hz), 7.89 (m, 6H), 7.45 (d, 6H, J = 8.65 Hz), 7.34 (m, 3H); MALDI-TOF MS: m/z 878.1.

Acknowledgements

The authors are thankful for the financial support from the National Nature Sciences Foundation of China (No. 51003118, 50973128, 61007066), the research programs from the Ministry of Science and Technology of China (No. 2009BAK64B03, 2012BAK07B03), the Shanghai Science and Technology Committee (No. 11JC1414700).

Notes and references

1 M. Dalene and G. Skarping, *J. Chromatogr., A*, 1985, **331**, 321.
2 S. Laha and R. G. Luthy, *Environ. Sci. Technol.*, 1990, **24**, 363.
3 T. Gao, E. S. Tillman and N. S. Lewis, *Chem. Mater.*, 2005, **17**, 2904.
4 (*a*) Y. K. Che, X. M. Yang, S. Loser and L. Zang, *Nano Lett.*, 2008, **8**, 2219; (*b*) B. P. Jiang, D. S. Guo and Y. Liu, *J. Org. Chem.*, 2011, **76**, 6101.
5 R. Prasad, R. Kumar and S. Prasad, *Anal. Chim. Acta*, 2009, **646**, 97.
6 C. He, Q. G. He, C. M. Deng, L. Q. Shi, D. F. Zhu, Y. Y. Fu, H. M. Cao and J. G. Cheng, *Chem. Commun.*, 2010, **46**, 7536.
7 J. R. Johnson, D. Karlsson, M. Dalene and G. Skarping, *Anal. Chim. Acta*, 2010, **678**, 117.
8 L. M. Games and R. A. Hites, *Anal. Chem.*, 1977, **49**, 1433.
9 J. L. Wang, G. D. Wang, G. A. S. Ansari and M. F. Khan, *Toxicol. Appl. Pharmacol.*, 2008, **230**, 227.
10 W. Wei, H. J. Wang and C. Q. Jiang, *Spectrochim. Acta, Part A*, 2008, **70**, 362.
11 X. L. Chen, Z. B. Li, Y. X. Zhu and J. G. Xu, *Anal. Chim. Acta*, 2004, **505**, 283.
12 J. S. Chiang and S. D. Huang, *Talanta*, 2008, **75**, 70.
13 J. F. Peng, J. F. Liu, G. B. Jiang, C. Tai and M. J. Huang, *J. Chromatogr., A*, 2005, **1072**, 3.
14 X. H. Wu, Z. G. Lei, Q. S. Li, J. Q. Zhu and B.H., *Ind. Eng. Chem. Res.*, 2010, **49**, 2581.
15 L. Muller, E. Fattore and E. Benfenati, *J. Chromatogr., A*, 1997, **791**, 221.
16 T. Spataru, N. Spataru and A. Fujishima, *Talanta*, 2007, **73**, 404.
17 E. H. Seymour, N. S. Lawrence, E. L. Beckett, J. Davis and R. G. Compton, *Talanta*, 2002, **57**, 233.
18 S. Y. Ai, M. N. Gao, W. Zhang, Q. J. Wang, Y. F. Xie and L. T. Jin, *Talanta*, 2004, **62**, 445.
19 S. W. Thomas, G. D. Joly and T. M. Swager, *Chem. Rev.*, 2007, **107**, 1339.
20 J. S. Yang and T. M. Swager, *J. Am. Chem. Soc.*, 1998, **120**, 11864.
21 G. V. Zyryanov, M. A. Palacios and P. Anzenbacher, *Org. Lett.*, 2008, **10**, 3681.
22 E. M. Nolan and S. J. Lippard, *Chem. Rev.*, 2008, **108**, 3443.
23 D. Aldakov, M. A. Palacios and P. Anzenbacher, *Chem. Mater.*, 2005, **17**, 5238.
24 A. Sassolas, B. D. Leca-Bouvier and L. J. Blum, *Chem. Rev.*, 2008, **108**, 109.
25 K. Y. Pu and B. Liu, *J. Phys. Chem. B*, 2010, **114**, 3077.
26 Q. Zou and H. Tian, *Sens. Actuators, B*, 2010, **149**, 20.
27 L. T. Zeng, P. F. Wang, H. Y. Zhang, X. Q. Zhuang, Q. Dai and W. M. Liu, *Org. Lett.*, 2009, **11**, 4294.
28 E. W. Miller, A. E. Albers, A. Pralle, E. Y. Isacoff and C. J. Chang, *J. Am. Chem. Soc.*, 2005, **127**, 16652.
29 R. Hu, J. A. Feng, D. H. Hu, S. Q. Wang, S. Y. Li, Y. Li and G. Q. Yang, *Angew. Chem., Int. Ed.*, 2010, **49**, 4915.
30 W. W. Li, C. Du, F. H. Li, Y. Zhou, M. Fahlman, Z. S. Bo and F. L. Zhang, *Chem. Mater.*, 2009, **21**, 5327.
31 K. Y. Pu and B. Liu, *Adv. Funct. Mater.*, 2009, **19**, 277.
32 P. Anant, N. T. Lucas and J. Jacob, *Org. Lett.*, 2008, **10**, 5533.
33 K. M. Omer, S. Y. Ku, K. T. Wong and A. J. Bard, *J. Am. Chem. Soc.*, 2009, **131**, 10733.
34 M. Akhtaruzzaman, M. Tomura, J. Nishida and Y. Yamashita, *J. Org. Chem.*, 2004, **69**, 2953.
35 E. J. Xu, H. L. Zhong, J. P. Du, D. L. Zeng, S. J. Ren, J. Sun and Q. Fang, *Dyes Pigm.*, 2009, **80**, 194.
36 S. Kato, T. Matsumoto, T. Ishi, T. Thiemann, M. Shigeiwa, H. Gorohmaru, S. Maeda, Y. Yamashita and S. Mataka, *Chem. Commun.*, 2004, 2342.
37 J. M. Lupton, I. D. W. Samuel, P. L. Burn and S. Mukamel, *J. Phys. Chem. B*, 2002, **106**, 7647.
38 J. C. Collings, S. Y. Poon, C. L. Droumaguet, M. Charlot, C. Katan, L. O. Palsson, A. Beeby, J. A. Mosely, H. M. Kaiser, D. Kaufmann, W. Y. Wong, M. Blanchard-Desce and T. B. Marder, *Chem.–Eur. J.*, 2009, **1**, 198.
39 C. Katan, F. Terenziani, O. Mongin, M. H. V. Werts, L. Porres, T. Pons, J. Mertz, S. Tretiak and M. Blanchard-Desce, *J. Phys. Chem. A*, 2005, **109**, 3024.
40 T. Suzuki, H. Fujii, Y. Yamashita, C. Kabuto, S. Tanaka, M. Harasawa, T. Mukai and T. Miyashi, *J. Am. Chem. Soc.*, 1992, **114**, 3034.
41 E. Kavitha, N. Sundaraganesan and S. Sebastian, *Indian J. Pure & Appl. Phys.*, 2010, **48**, 20.
42 C. M. Deng, P. Gong, Q. G. He, J. G. Cheng, C. He, L. Q. Shi, D. F. Zhu and T. Lin, *Chem. Phys. Lett.*, 2009, **483**, 219.
43 D. F. Zhu, Q. G. He, Q. Chen, Y. Y. Fu, C. He, L. Q. Shi, X. Meng, H. M. Cao and J. G. Cheng, *ACS Nano*, 2011, **5**, 4293.